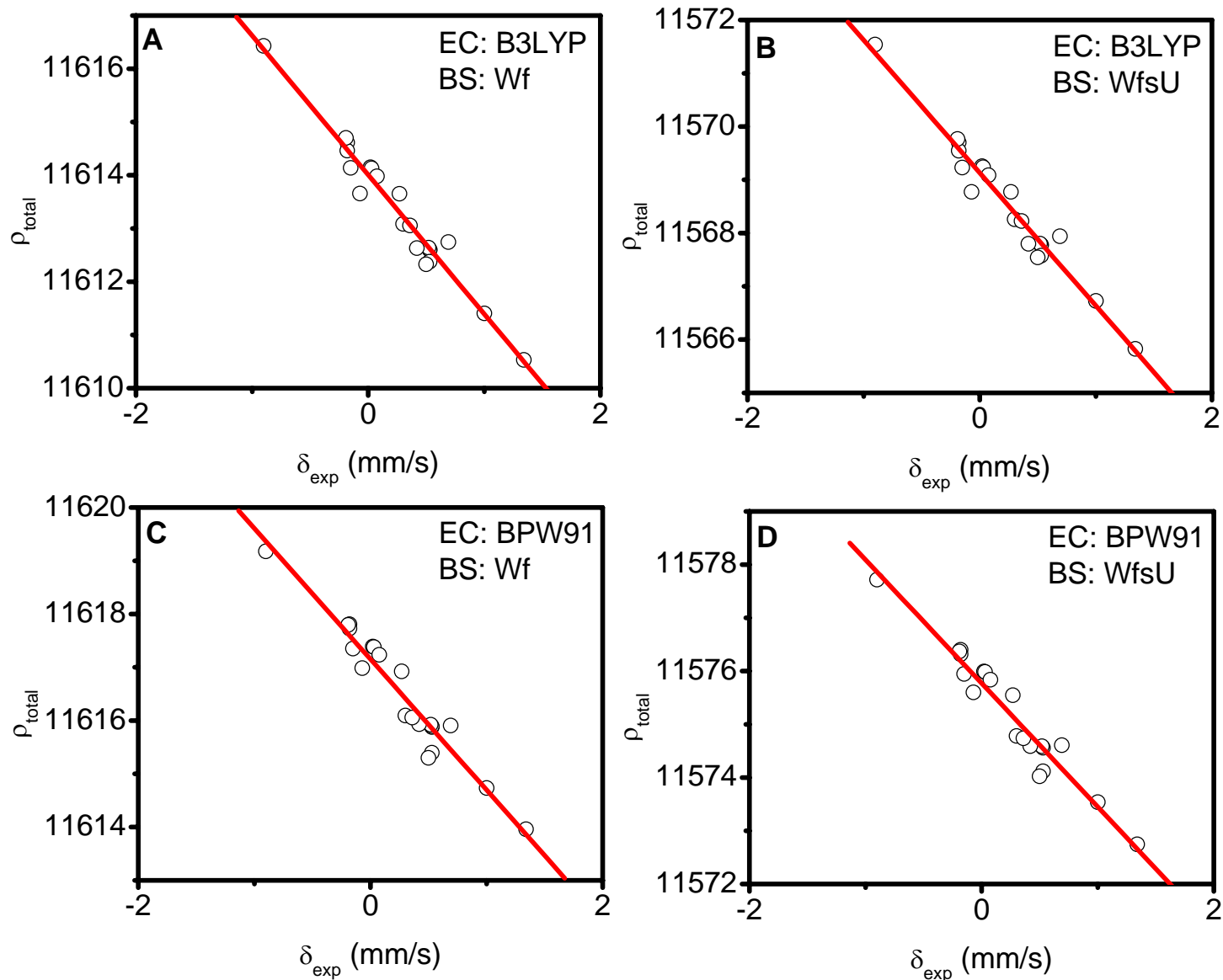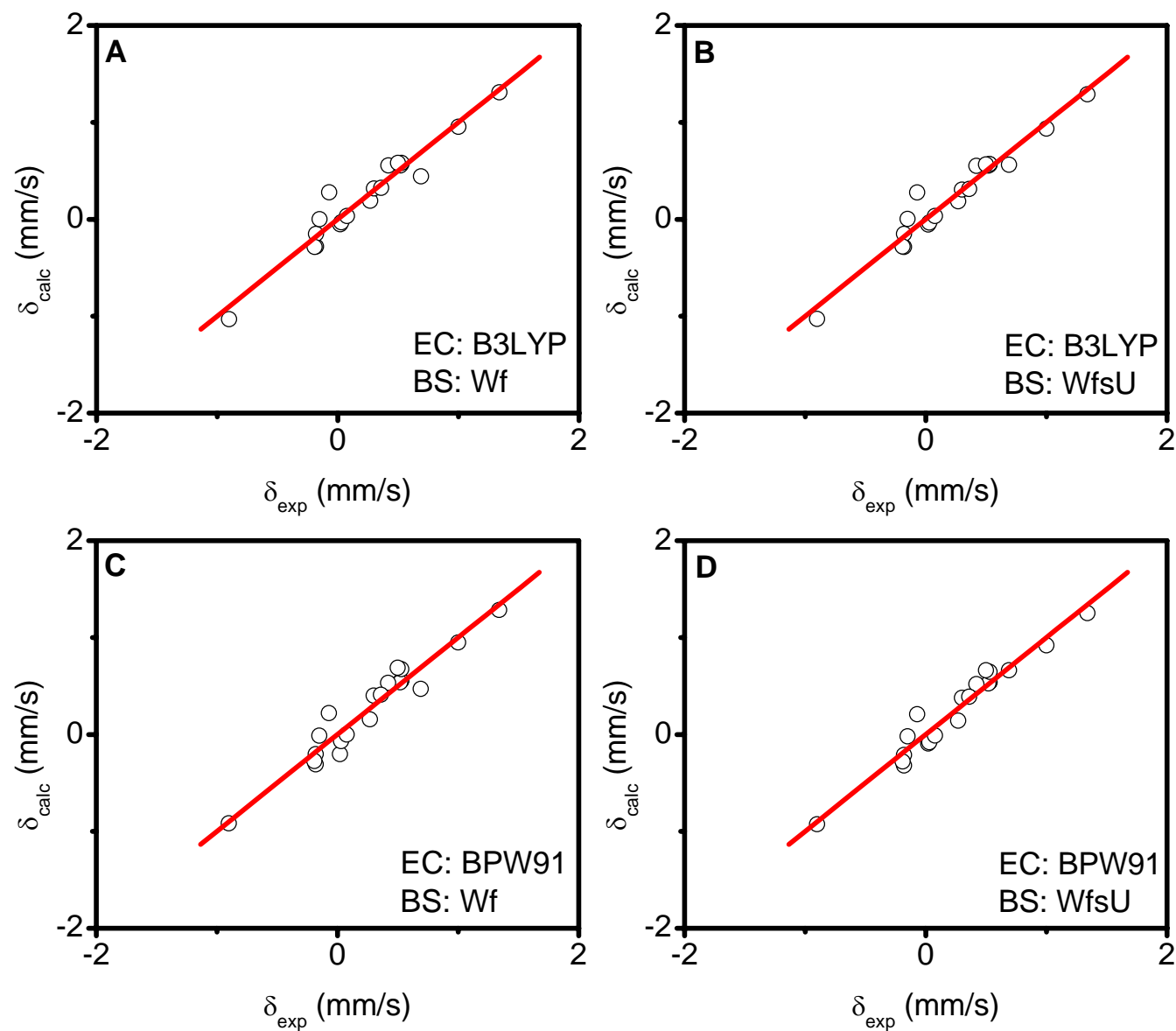**Supporting Information Figure 1.** Correlation between experimental isomer shifts (δ_{exp}) and calculated (B3LYP geometry test set) total electron density at the ^{57}Fe nucleus (ρ_{total}) using: **(A)** B3LYP functional and Wf basis set; **(B)** B3LYP functional and WfsU basis set; **(C)** BPW91 functional and Wf basis set; **(D)** BPW91 functional and WfsU basis set.

Nemykin & Hadt

Supporting Information Figure 2. Correlation between experimental isomer shifts (δ_{exp}) and calculated (BP86 geometry test set) total electron density at the ^{57}Fe nucleus (ρ_{total}) using: **(A)** B3LYP functional and Wf basis set; **(B)** B3LYP functional and WfsU basis set; **(C)** BPW91 functional and Wf basis set; **(D)** BPW91 functional and WfsU basis set.
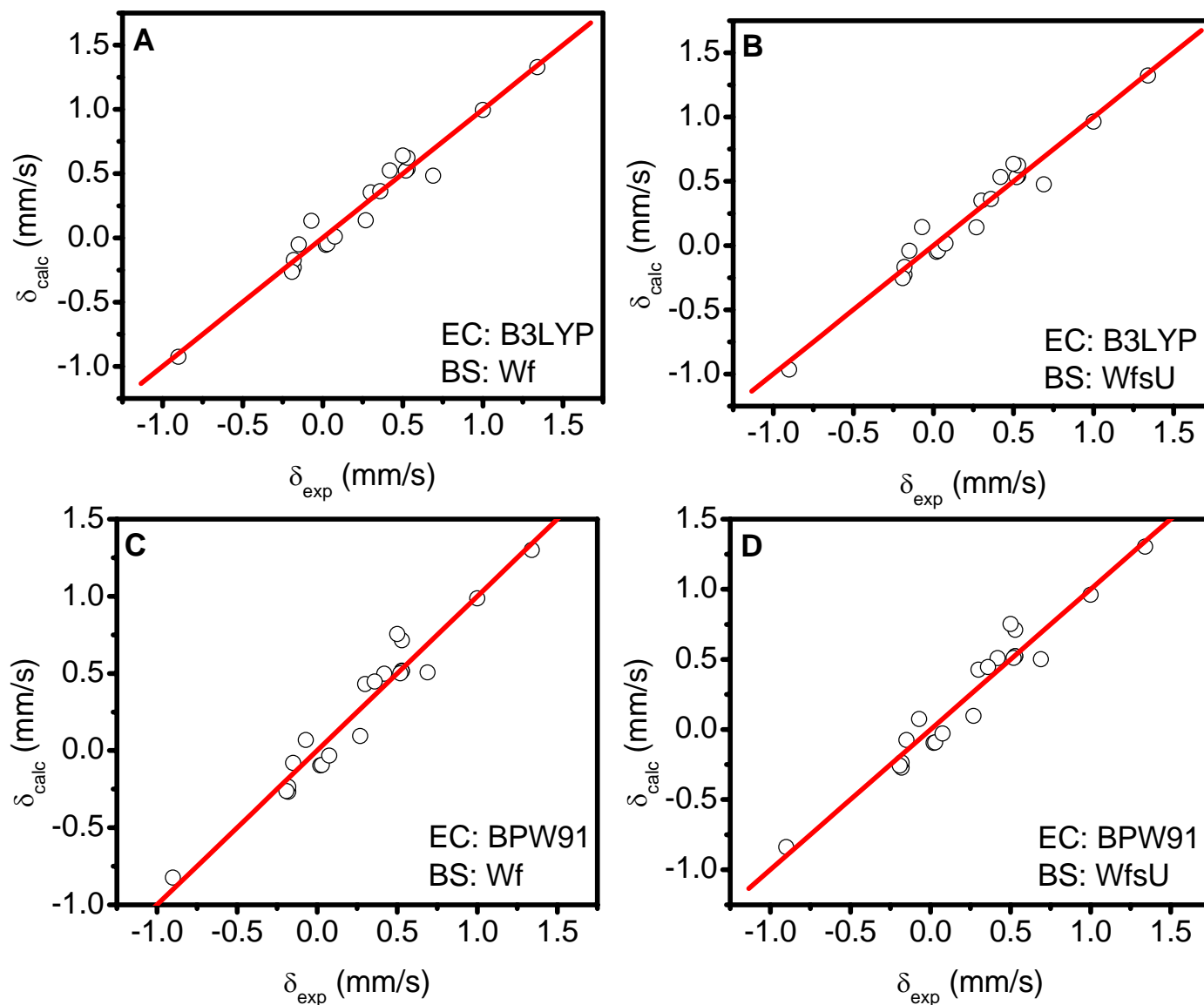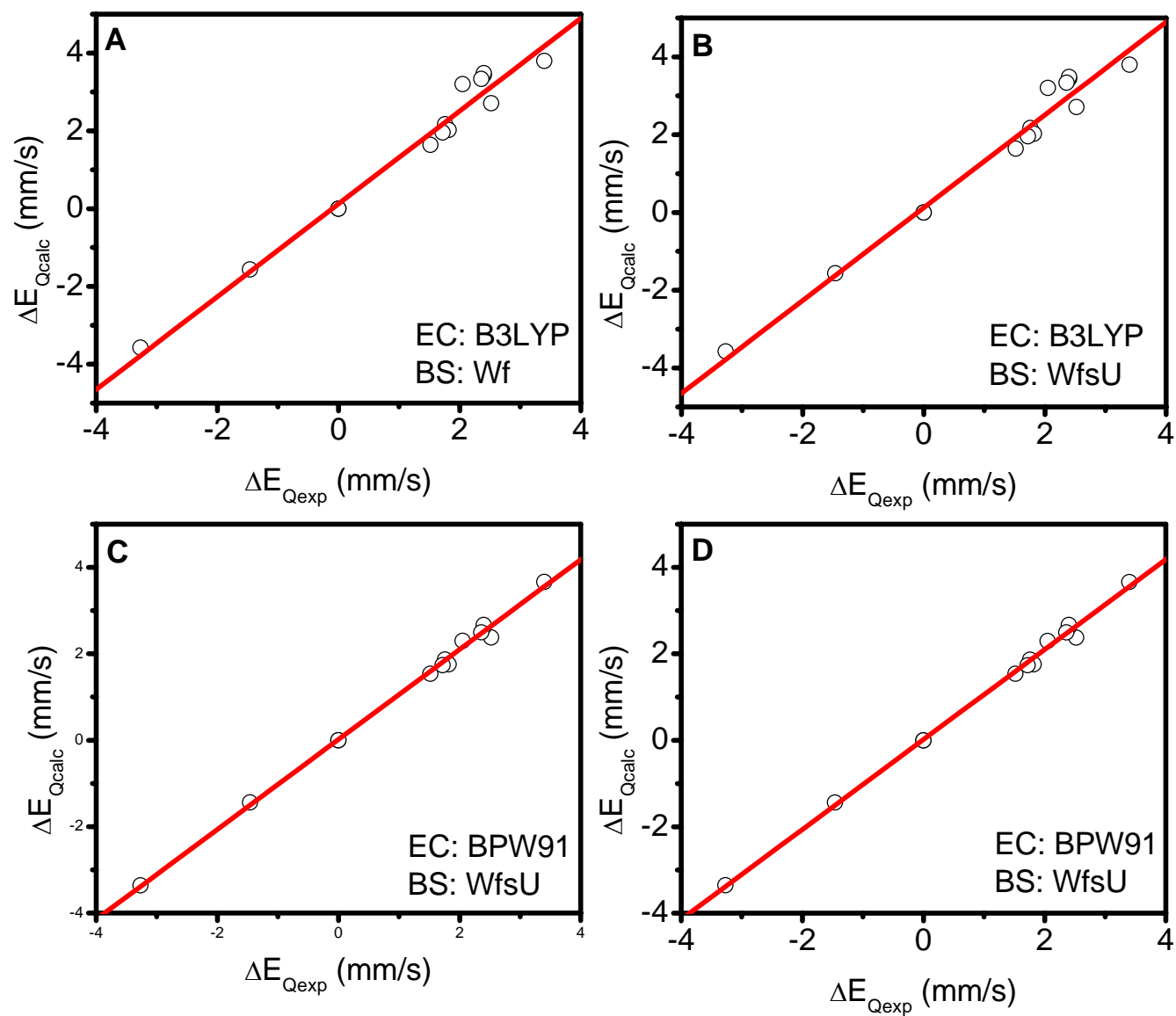
Nemykin & Hadt

Supporting Information Figure 3. Correlation between experimental (δ_{exp}) and calculated (δ_{calc}) isomer shifts (B3LYP geometry test set) using: **(A)** B3LYP functional and Wf basis set; **(B)** B3LYP functional and WfsU basis set; **(C)** BPW91 functional and Wf basis set; **(D)** BPW91 functional and WfsU basis set.
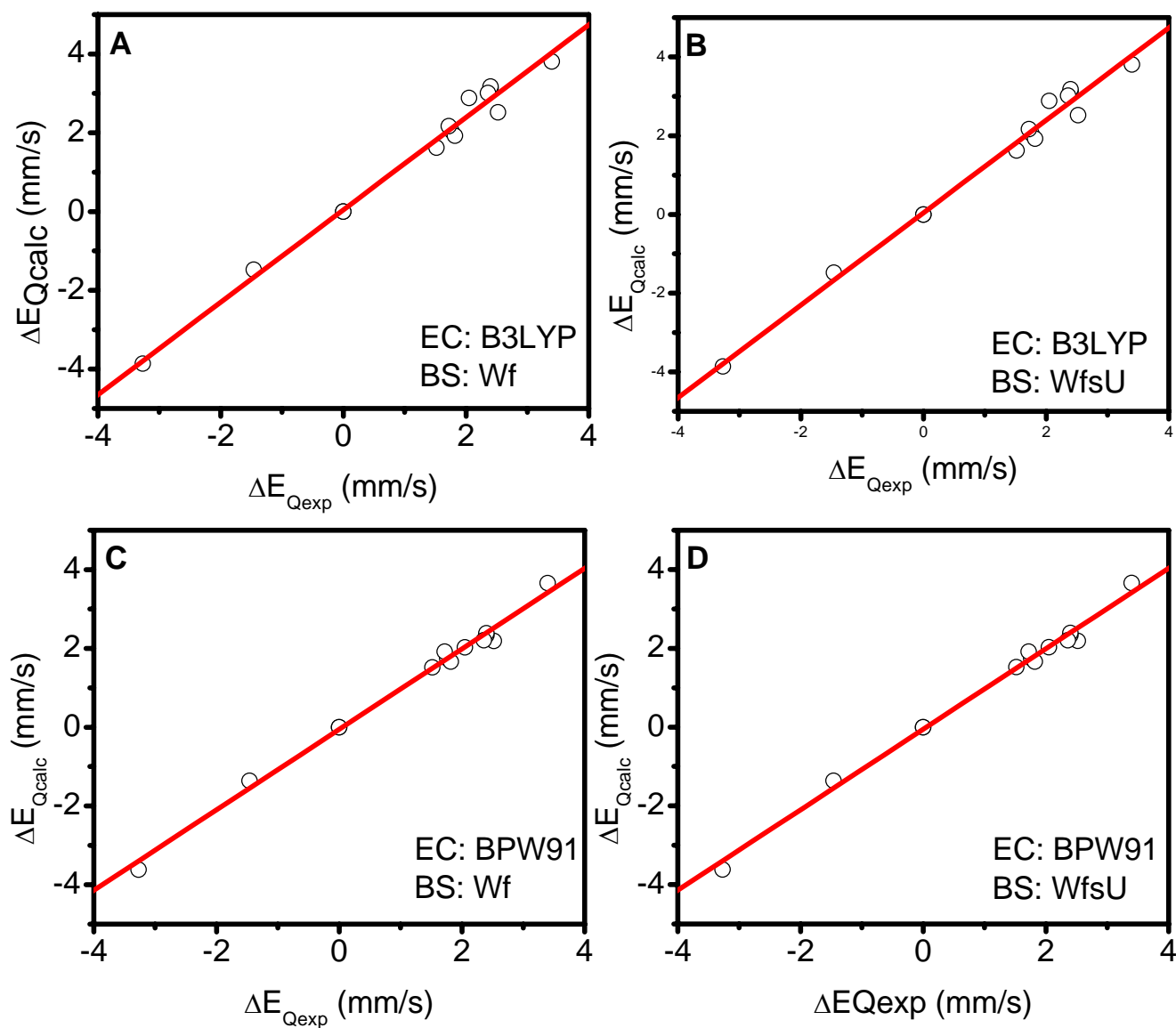
Nemykin & Hadt

Supporting Information Figure 4. Correlation between experimental (δ_{exp}) and calculated (δ_{calc}) isomer shifts (BP86 geometry test set) using: **(A)** B3LYP functional and Wf basis set; **(B)** B3LYP functional and WfsU basis set; **(C)** BPW91 functional and Wf basis set; **(D)** BPW91 functional and WfsU basis set.

Nemykin & Hadt

Supporting Information Figure 5. Correlation between experimental (ΔE_{Qexp}) and calculated (ΔE_{Qcalc}) quadrupole splittings (B3LYP geometry test set) using: **(A)** B3LYP functional and Wf basis set; **(B)** B3LYP functional and WfsU basis set; **(C)** BPW91 functional and Wf basis set; **(D)** BPW91 functional and WfsU basis set.
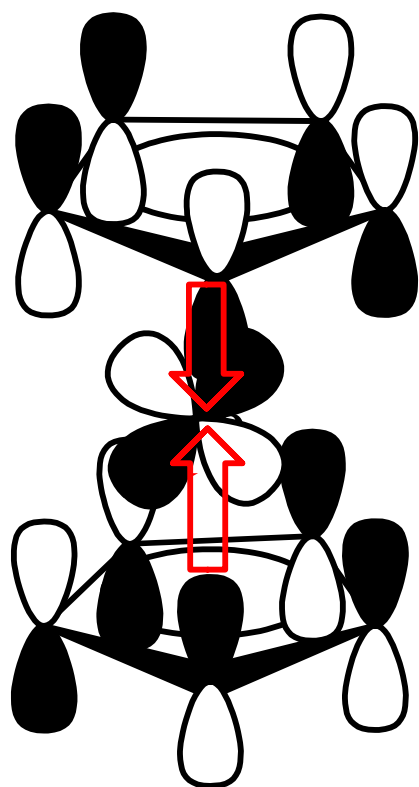
Nemykin & Hadt

Supporting Information Figure 6. Correlation between experimental (ΔE_{Qexp}) and calculated (ΔE_{Qcalc}) quadrupole splittings (BP86 geometry test set) using: **(A)** B3LYP functional and Wf basis set; **(B)** B3LYP functional and WfsU basis set; **(C)** BPW91 functional and Wf basis set; **(D)** BPW91 functional and WfsU basis set.
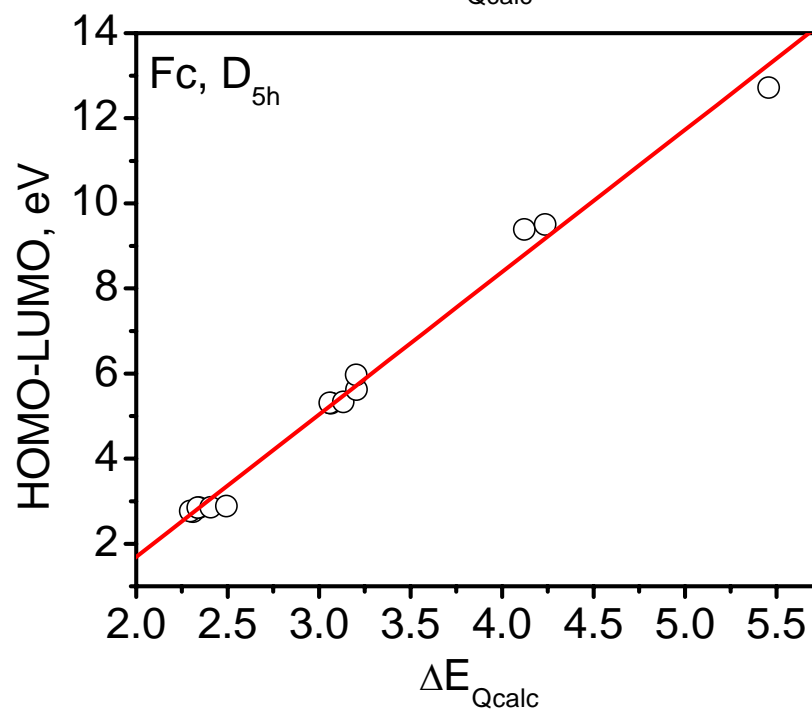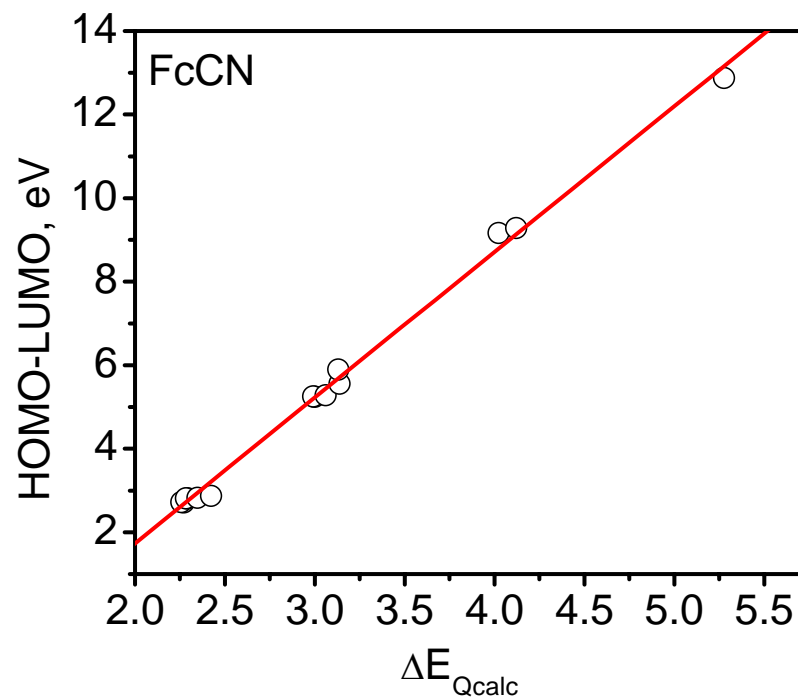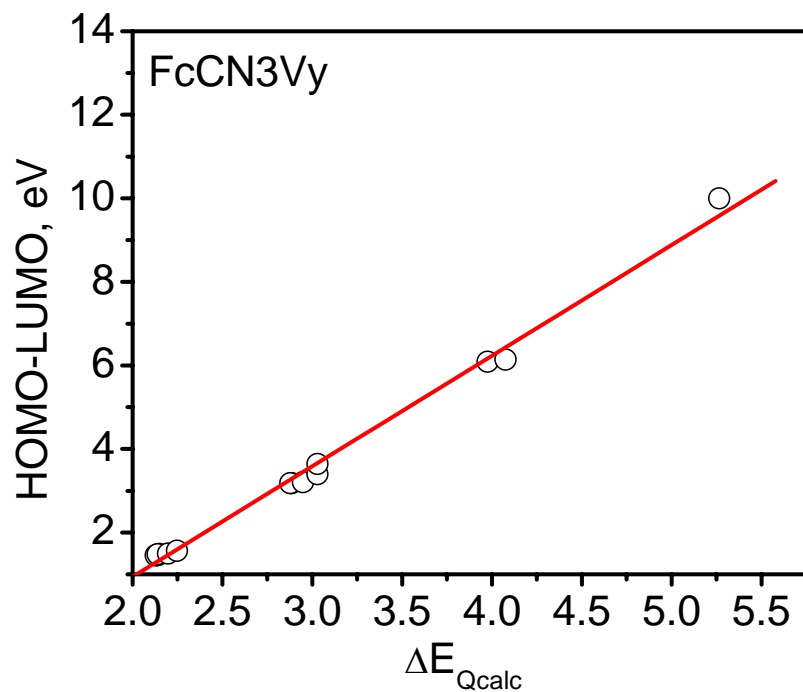
Nemykin & Hadt
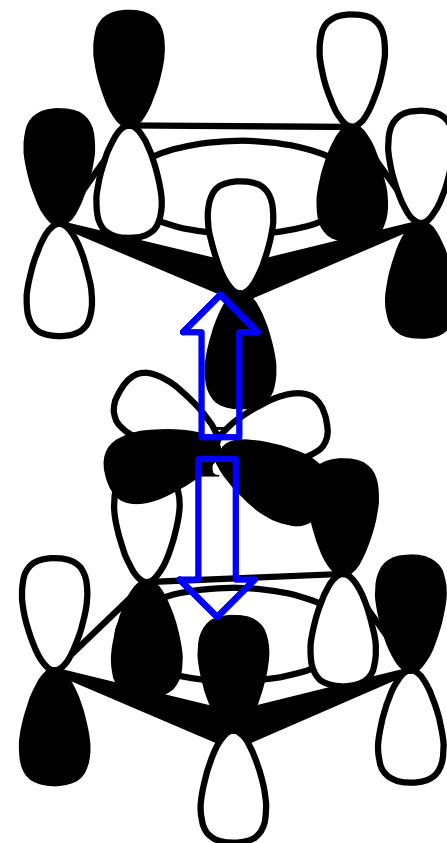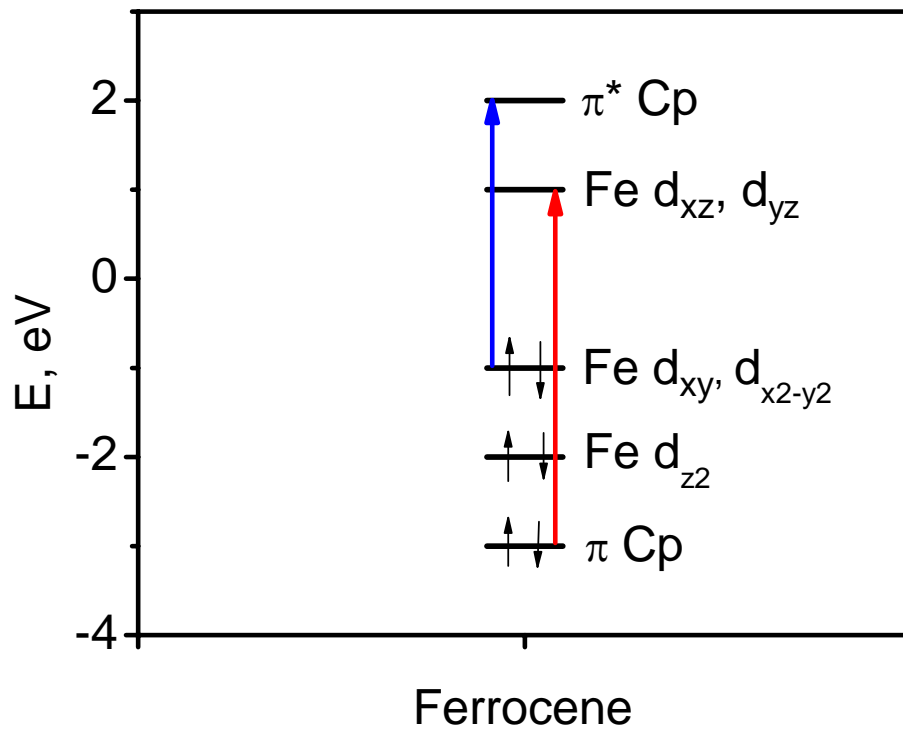
Supporting Information Figure 7. Bonding interactions between Cp⁻ ligand and Fe^{II} ion in ferrocene along with charge-transfer transitions.

Nemykin & Hadt

Supporting Information Figure 8. Correlation between calculated quadrupole splittings and HOMO-LUMO energy gap in ferrocene (Fc), cyanoferrocene (FcCN), and tricyanovinylferrocene (FcCN3Vy).

Nemykin & Hadt
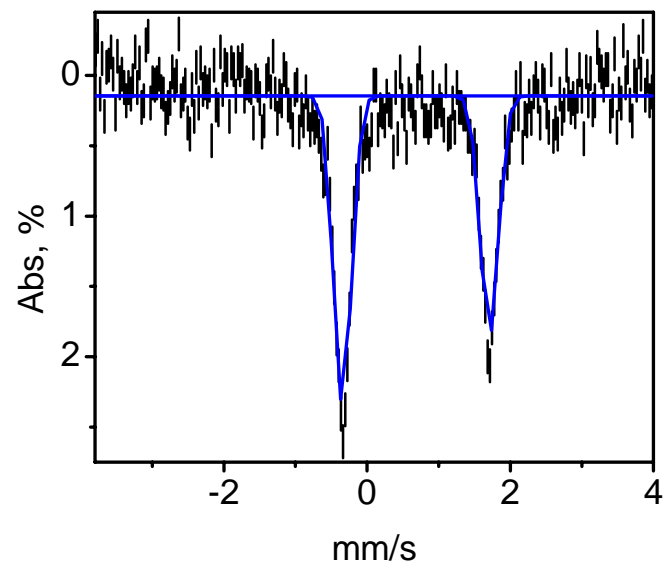
Room-temperature Mössbauer spectrum of $FcCN_3Vy$. Spectrum was recorded using NGRS-4 spectrometer in constant acceleration mode and referenced to sodium nitroprusside at room-temperature. The source was [57]Co in a chromium matrix with initial activity of 50 mCi.

Nemykin & Hadt

Supporting Information Table 1. Comparison of correlation coefficients (r) and α_{rel} for the test sets which utilize -0.18 mm/s and 0.00 mm/s (in parenthesis) values for isomer shift in $Fe(CO)_5$ complex.

	BPW91/Wf	BPW91/WfsU	B3LYP/Wf	B3LYP/WfsU
	Method			
	X-ray geometry			
r	0.978(0.975)	0.977(0.974)	0.987(0.986)	0.985(0.983)
α_{rel}	-0.337(-0.335)	-0.357(-0.353)	-0.304(-0.301)	-0.320(-0.317)
	B3LYP geometry			
r	0.965(0.961)	0.975(0.970)	0.969(0.967)	0.974(0.972)
α_{rel}	-0.308(-0.305)	-0.320(-0.317)	-0.291(-0.288)	-0.303(-0.300)
	BP86 geometry			
r	0.971(0.966)	0.971(0.966)	0.981(0.978)	0.980(0.978)
α_{rel}	-0.313(-0.311)	-0.331(-0.329)	-0.294(-0.291)	-0.308(-0.305)